Over-the-Air Transmission of Zak-OTFS with Spread Pilots on Sub-THz Communications Testbed

Claire Parisi†, Venkatesh Khammammetti*, Robert Calderbank*, and Lauren Huie†
*Electrical and Computer Engineering Department, Duke University, Durham, NC, USA
†Information Directorate, Air Force Research Laboratory, Rome, NY, USA
claire.parisi@us.af.mil, venkatesh.khammammetti@duke.edu, robert.calderbank@duke.edu, and lauren.huie-seversky@us.af.mil

***Abstract*—Looking towards 6G wireless systems, frequency bands like the sub-terahertz (sub-THz) band (100 GHz - 300 GHz) are gaining traction for their promises of large available swaths of bandwidth to support the ever-growing data demands. However, challenges with harsh channel conditions and hardware nonlinearities in the sub-THz band require robust communication techniques with favorable properties, such as good spectral efficiency and low peak-to-average power ratio (PAPR). Recently, OTFS and its variants have garnered significant attention for their performance in severe conditions (like high delay and Doppler), making it a promising candidate for future communications. In this work, we implement Zak-OTFS for the over-the-air experiments with traditional point pilots and the new spread pilots. Notably, we design our spread-pilot waveforms with communications and sensing coexisting in the same radio resources. We define the system model and the signal design for integration onto our state-of-the-art sub-THz wireless testbed. We show successful data transmission over-the-air at 140 GHz and 240 GHz in a variety of signal-to-noise ratio (SNR) conditions. In addition, we demonstrate integrated sensing and communications (ISAC) capabilities and show PAPR improvement of over 5 dB with spread pilots compared to point pilots.**

***Index Terms*—delay-Doppler, ISAC, OTFS, PAPR, sub-THz, spread-pilots**

I. Introduction

To meet the demand for ultra-high data rates in next-generation wireless systems, attention has turned towards emerging spectral, such as the sub-terahertz (sub-THz) band (100 GHz - 300 GHz), with large contiguous swaths of bandwidth capable of supporting high-data, wideband applications. While systems in this band have already shown great promise [1], [2], these frequencies come with a unique set of challenges, including higher path losses, Doppler spread, and suceptibilty to phase noise and peak-to-average power ratio (PAPR) [3], [4]. Orthogonal Time Frequency Space (OTFS), as presented in [5], is an emerging waveform candidate designed specifically to overcome harsh channel conditions through strategic design and resource allocation in the delay-Doppler (DD) domain. Inherent properties grant OTFS significant advantages in high-mobility scenarios and challenging propagation environments, such as the sub-THz regime, by making the input-output (I/O) relationship predictable. Previous studies in [6], [7] show that OTFS and spread-variations on OTFS show potential in the context of sub-THz band hardware and channel challenges. Specifically, OTFS often shows improved performance over Orthogonal Frequency Division Multiplexing (OFDM), a technique that is widely used in current 5G and LTE systems, in a variety of studies and scenarios [8]–[10]. However, OTFS suffers from high PAPR, making spread variations attractive candidates (like spread pilots, which reduce PAPR through filtering) [11]. Zak-OTFS is a new variant of OTFS [12] that is designed to make the I/O relation predictable even when the propagation environment is harsh, and it can also reduce the PAPR [11]. In addition, future wireless systems in 6G and beyond are projected to support artificial intelligence/machine learning (AI/ML) and integrated sensing and communications (ISAC) capabilities [2], making OTFS an even more advantageous technique since it generates a time-invariant channel representation (better for training AI/ML models) and supports the overlay of sensing and communications resources in the same frame.

As such, in this paper, we focus our attention on the implementation of Zak-OTFS system with both point and spread pilots on practical sub-THz hardware to showcase feasibility for next-generation communications systems. We design time domain (TD) OTFS packets in software using our Zak-OTFS transmitter and receiver models. We model two different packets, one using point pilots (where the data frame is proceeded by the pilot frame) and a second for ISAC (where the spread pilots and data are overlayed within the same frame). From there, we integrate our waveforms onto universal software radio peripheral (USRP) B210 radios connected to sub-THz frontends to transmit both waveforms over-the-air at 140 GHz and 240 GHz. We successfully demonstrate data transmission and sensing capabilities on the sub-THz testing setup. We see promising performance of Zak-OTFS in a variety of signal-to-noise ratio (SNR) scenarios and demonstrate preliminary ISAC capabilities in addition to reduced-PAPR with spread pilots.

The remainder of this paper is organized as follows: in Section II, we describe the system design details of Zak-OTFS; in Section III we overview our sub-THz testing hardware setup; in Section IV, we discuss how we integrate our OTFS design onto the testbed; in Section V, we showcase the results of wireless transmission of Zak-OTFS with point pilots and

This work was supported by the NSF (2342690, 2342690, and 214821), the AFOSR (FA8750-20-2-0504 and FA9550-23-1-0249), and by funds from federal agency and industry partners as specified in the Resilient & Intelligent NextG Systems (RINGS) program.

spread pilots; lastly, we conclude in Section VI

II. OTFS System Design

For our OTFS transceiver design, we choose Zak-OTFS (also referred to as OTFS 2.0) [12] as our model. Zak-OTFS transforms the two dimensional (2D) DD signal directly into the TD using the Zak transform, which is proven to be more robust to channel delay and Doppler spreads, more effective in predicting the I/O relation and has good spectral efficiency performance compared to other versions of OTFS (like the most studied MC-OTFS) [13]. When implementing Zak-OTFS systems with a point pilot, we introduce a guard band around the pilot location, within which no data is transmitted to get an efficient channel prediction to equalize on the data. However, this decreases the overall spectral efficiency and also has has high PAPR, because of the point pilots. To overcome these issues, the spread-pilot-based channel prediction technique is introduced in [11]. The remainder of this section describes the Zak-OTFS system (transmitter and receiver) used for the over-the-air experimentation on the sub-THz bands and also explains the point pilot and spread pilot.

A. Zak-OTFS Transmitter

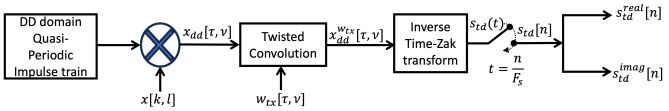

Fig. 1: Zak-OTFS baseband Modulation

Consider the fundamental periods of the DD domain to be τ_p along delay and ν_p along the Doppler domains, ($\tau_p \cdot \nu_p = 1$). The delay and Doppler periods are sub-divided into M and N equal parts, respectively, such that each DD resolution is $\left(\frac{\tau_p}{M} = \frac{1}{B}, \frac{\nu_p}{N} = \frac{1}{T}\right)$, where B and T are the bandwidth and time duration of the Zak-OTFS signal. The MN information symbols $x[k,l]$, $k = 0, 1, ..., M-1$, $l = 0, 1, ..., N-1$ are mapped onto the MN DD resolutions in the fundamental domain such that $x[k,l] = x[k\tau_p/M, l\nu_p/N]$. From [12] and the properties of the Zak transform, the DD input signal to the inverse Zak transform should be quasi-periodic[1] in nature. From [12], the quasi-periodic continuous DD domain signal is defined as

$$x_{\text{dd}}(\tau,\nu) \triangleq \sum_{k,l\in\mathbb{Z}} x_{\text{dd}}[k,l]\,\delta(\tau - k/B)\,\delta(\nu - l/T),$$

$$x_{\text{dd}}[k+nM, l+mN] \triangleq x[k,l]e^{j2\pi n\frac{l}{N}},\ m,n\in\mathbb{Z}. \quad (1)$$

From Fig.1, the output of the twisted convolution is given by

$$\begin{aligned} x_{\text{dd}}^{w_{tx}}(\tau,\nu) &= w_{tx}(\tau,\nu)\ *_\sigma\ x_{\text{dd}}(\tau,\nu) \\ &= \iint w_{tx}(\tau',\nu')\,x_{dd}(\tau-\tau',\nu-\nu') \\ &\qquad e^{j2\pi\nu'(\tau-\tau')}d\tau' d\nu' \quad (2) \end{aligned}$$

[1]quasi-periodic means periodic with a phase shift

In this paper, we consider 2D DD 'sinc' filter, $w_{tx}(\tau,\nu) \triangleq \sqrt{BT}\,\text{sinc}(B\tau)\,\text{sinc}(T\nu)$ (refer [13]–[15] for other DD filters). Substituting (1) and $w_{tx}(\tau,\nu)$ in (2) gives

$$\begin{aligned} x_{\text{dd}}^{w_{tx}}(\tau,\nu) &= \sqrt{BT}\sum_{k,l\in\mathbb{Z}} x_{\text{dd}}[k,l]\ \ \text{sinc}\left(T(\nu-\frac{l}{T})\right) \\ &\qquad \text{sinc}\left(B(\tau-\frac{k}{B})\right)e^{j2\pi\left(\nu-\frac{l}{T}\right)\frac{k}{B}} \quad (3) \end{aligned}$$

Applying the inverse time Zak transform on $x_{\text{dd}}^{w_{tx}}(\tau,\nu)$ (see Fig. 1) results in a physical TD signal $s_{\text{td}}(t)$ [12], i.e.,

$$s_{\text{td}}(t) = \sqrt{\tau_p}\int_0^{\nu_p} x_{\text{dd}}^{w_{tx}}(t,\nu)d\nu \quad (4)$$

Substituting (3) in (4) (see [16] for the detailed derivation) gives,

$$\begin{aligned} s_{\text{td}}(t) &= \sqrt{\frac{B\tau_p}{T}}\sum_{k=0}^{M-1}\sum_{l=0}^{N-1} x[k,l]\left[\sum_{n=-\frac{N}{2}}^{\frac{N}{2}-1} e^{j2\pi\frac{nl}{N}}\right. \\ &\qquad \left.\text{sinc}\left(B\left(t-n\tau_p-\frac{k\tau_p}{M}\right)\right)\right] \quad (5) \end{aligned}$$

Now the complex TD signal $s_{\text{td}}(t)$ is sampled at a sampling rate $F_s \geq B$, where B is the Nyquist rate. Therefore, the q-th sample obtained by sampling $s_{\text{td}}(t)$ at $t = q/F_s$ is given by

$$\begin{aligned} s_{\text{td}}[q] &\triangleq s_{\text{td}}\left(t = q/F_s\right) = \sqrt{\frac{B\tau_p}{T}}\sum_{k=0}^{M-1}\sum_{l=0}^{N-1} x[k,l] \\ &\qquad \left[\sum_{n=-\frac{N}{2}}^{\frac{N}{2}-1} e^{j2\pi\frac{nl}{N}}\,\text{sinc}\left(B\left(\frac{q}{F_s}-n\tau_p-\frac{k\tau_p}{M}\right)\right)\right] \quad (6) \end{aligned}$$

Since $s_{\text{td}}(t)$ has time duration T and lies in the interval $[-T/2, T/2)$, $s_{\text{td}}[q]$ takes non-zero values only for $q = -\frac{F_sT}{2}, \cdots, \frac{F_sT}{2}$, i.e., roughly F_sT samples.

B. Zak-OTFS Receiver

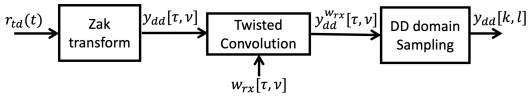

Fig. 2: Zak-OTFS baseband Demodulation

At the receiver, a time Zak transform is applied to the received baseband TD signal $r_{\text{td}}(t)$ to obtain a 2D DD signal $y_{\text{dd}}(\tau,\nu)$ (See Fig. 2). This signal ($y_{\text{dd}}(\tau,\nu)$) is twisted convolved with the DD receiver pulse shaping filter $w_{rx}(\tau,\nu)$ to get $y_{\text{dd}}^{w_{rx}}$. The DD sampled signal $y_{\text{dd}}[k,l]$ is obtained by sampling $y_{\text{dd}}^{w_{rx}}(\tau,\nu)$ at $\tau = k\frac{\tau_p}{M}, \nu = l\frac{\nu_p}{N}$. The entire process of converting the received baseband signal $r_{\text{td}}(t)$ to DD a sampled signal $y_{\text{dd}}[k,l]$ (see Fig. 2) can be done in two steps.

1) In the first step,the received baseband TD signal $r_{\text{td}}(t)$ is passed through an ideal low-pass filter (LPF) and the filtered output is given by

$$y(t) = r_{\text{td}}(t) * (B\,\text{sinc}(Bt)) = B\int \text{sinc}(B\tau)r_{\text{td}}(t-\tau)d\tau \quad (7)$$

Now limiting the TD signal $y(t)$ to the TD interval $[-T/2, T/2]$ collect the samples at sampling rate B such that $y[n] = y\left(t = \frac{n}{B}\right)$.

2) In the second step, apply discrete time Zak transform (DZT) to convert the discrete-time signal $y[n]$ to the discrete-DD domain signal $y_{\text{dd}}[k,l]$, i.e.,

$$y_{\text{dd}}[k,l] = \sum_{n=-\frac{N-1}{2}}^{\frac{N-1}{2}} y[k+nM]e^{-j2\pi\frac{nl}{N}}, \quad k=0,1,\cdots,M-1, l=0,1,\cdots,N-1. \tag{8}$$

Note that step one of this two-step process is only valid if the receiver pulse shaping filter is sinc i.e., $w_{rx}(\tau,\nu) = \sqrt{BT}\,\text{sinc}(B\tau)\,\text{sinc}(T\nu)$.

The DD received signal $y_{\text{dd}}[k,l]$ is the twisted convolution of the effective DD domain channel filter $h_{\text{eff}}[k,l]$ with the input, and the channel filter $h_{\text{eff}}[k,l]$ is formally defined in [13]. Using $y_{\text{dd}}[k,l]$, we predict the effective discrete DD channel filter $h_{\text{eff}}[k,l]$. The maximum likelihood (ML) estimate of $h_{\text{eff}}[k,l]$ is then given by the cross-ambiguity between the received pilot signal $y_{\text{dd}}[k,l]$ and the transmitted pilot signal $x_{\text{i,dd}}[k,l]$ (refer [11] for more details), i.e.,

$$\widehat{h}_{\text{eff}}[k,l] = A_{y_s,x_s}[k,l] = \sum_{k'=0}^{M-1}\sum_{l'=0}^{N-1} y_{\text{dd}}[k',l']\, x^*_{\text{i,dd}}[k'-k,l'-l]\, e^{-j2\pi\frac{l(k'-k)}{MN}}, \tag{9}$$

for $(k,l)\in\mathcal{S}$, where $\mathcal{S}$ is the support set over which the DD channel spreads and $x_{\text{i,dd}}[k,l]$ can be point or spread pilot signal used during transmission. After estimating, $\widehat{h}_{\text{eff}}[k,l]\ \forall k,l$ we generate the predicted channel matrix, (as described in [13]), and perform minimum mean squared error (MMSE) equalization to estimate the transmitted information symbols.

C. Pilot signal

We predict the I/O relation from the pilot response (the data complicates prediction). For the experiments performed in this paper, we transmitted two types of pilots in the DD domain: 1) point pilot and 2) spread pilot.

1) Point Pilot: A symbol located at (k_p,l_p) in the DD domain. i.e., $x_{\text{p}}[k,l] = \delta[k-k_p]\delta[l-l_p]$. From the definition of quasi-peridocity (see (1)), the discrete quasi-periodic DD domain point pilot is given by

$$x_{\text{p,dd}}[k,l] = \sum_{n,m\in\mathbb{Z}} e^{j2\pi\frac{nl}{N}}\delta[k-k_p-nM]\delta[l-l_p-mN] \tag{10}$$

2) Spread Pilot: The DD domain signal obtained by MN-periodic twisted convolution of a MN-periodic discrete DD filter $w[k,l]$ with the discrete quasi-periodic signal $x_{\text{p,dd}}[k,l]$, i.e.,

$$x_{\text{s,dd}}[k,l] = w[k,l] \circledast_\sigma x_{\text{p,dd}}[k,l] \tag{11}$$

where $\circledast_\sigma$ denotes the MN-periodic twisted convolution defined in [11]. The MN-periodic discrete DD filter $w[k,l]$ is given by

$$w[k,l] = \frac{1}{MN}e^{j2\pi\frac{u\left(k^2+l^2\right)}{MN}}, \ \forall\ k,l\in\mathbb{Z}, \tag{12}$$

where $u\in\mathbb{Z}$ is the slope parameter. Substituting (12) in (11) gives

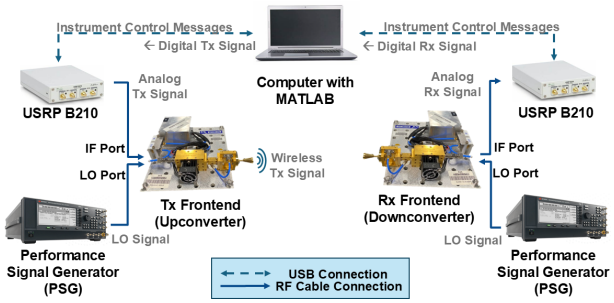

Fig. 3: Sub-THz testbed system diagram

$$x_{\text{s,dd}}[k,l] = \sum_{n=0}^{N-1}\sum_{m=0}^{M-1} e^{j2\pi n\frac{(l_p+mN)}{N}} e^{j2\pi\frac{(l-l_p-mN)(k_p+nM)}{MN}} w\left[k-k_p-nM, l-l_p-mN\right]. \tag{13}$$

In order to make $|x_{\text{s,dd}}[k,l]|$ almost constant for all (k,l), M and N should be odd primes and u should be relatively prime to both M and N. Also $\sum_{k=0}^{M-1}\sum_{l=0}^{N-1}|x_{\text{s,dd}}[k,l]|^2 = 1$. Also, other spread pilots, like ZC pilots defined in [17] can be used.

III. Sub-THz Testbed Overview

Transmitting within the sub-THz band requires the use of specially designed transmitter (Tx) and receiver (Rx) modules. We utilize two upconverter/downconverter pairs, one which operates at a center frequency of 140 GHz and another at 240 GHz. The 140 GHz frontends are custom-built mixer/amplifier/multiplier-chain (MixAMC) units from Virginia Diodes Inc. (VDI). The MixAMC has a multiplication factor of 12 and a WR-6.5 conical horn antenna with 13° half-power beamwidth. The 240 GHz frontends are commercial off-the-shelf compact converter up/down converters (CCU and CCD). The CCU and CCD units have a 6× multiplication factor and WR-4.3 conical horn antennas with 13 ° half-power beamwidth. Starting with the transmit side, the upconverter module is driven by an external local oscillator (LO) signal provided by Keysight performance signal generator (PSG). The PSG is a low-noise signal generator that operates up to 40 GHz, which provides a high enough frequency to drive our frontend systems given their multiplication factors. The LO gets multiplied and mixed with an intermediate frequency (IF) signal. In our case, this IF signal is our OTFS signal provided by a USRP. USRP B-210 models generate signals between 70 MHz up to 6 GHz and has an internal clock rate of up to 60 MHz. On the receive side, we similarly, connect a downconverter frontend to a PSG to supply the LO and a USRP for signal processing. Both transmit and receive USRPs are controlled by a laptop running MATLAB commands for automated control, leveraging Communications Toolbox Support Package for USRP Radio. Our testbed setup is shown in Fig. 4 and the connection diagram in Fig. 3.

IV. OTFS Implementation

To complete over-the-air experimentation, we must synthesize our signal processing and design with the wireless testbed

hardware and testing workflow. In this section, we detail our implementation and define the parameters of the experiment.

A. Baseband Signal Design & Processing

The TD transmit signals are packet-like, containing a header sequence for synchronization and recovery followed by the baseband Zak-OTFS signal. We used a three-segmented Zadoff-Chu sequence with different lengths as the header sequence to synchronize data and estimate carrier frequency offset (CFO) [18]. For the experiments in this paper, we designed two different baseband Zak-OTFS signals, one for point pilot case and the other for spread pilot case.

For the point pilot case, we transmit pilot and data in separate DD frames. In one DD frame, we transmit only point pilot at location $(k_p = \frac{M}{2}, l_p = \frac{N}{2})$ making other DD resources as zero and in the adjacent frame, we transmit the information symbols. We separately transform these DD frames into TD using Section II-A. We concatenate these two TD signals to create a baseband Zak-OTFS signal ready to sense and communicate. At the receiver, once syncronized, we deconcatenate and transform separately the pilot and data signal from TD to DD domain. The predicted DD channel from the received DD pilot signal is used to equalize the data in the data frame[2].

For the spread pilot case, we use (13) and $(k_p = \frac{M+1}{2}, l_p = \frac{N+1}{2})$[3] to create a DD spread signal which is added to the DD information symbols, and then the combined signal is transformed into TD to get the baseband Zak-OTFS signal [11]. Once syncronized at the receiver, we transform the TD signal to DD domain and use the combined, spread pilot plus data, signal to predict the channel. Now using the predicted channel, we remove the contribution of the spread pilot from the received DD signal to get the received DD data frame.

In both cases, point pilot and spread pilot, we predicted the DD channel by the cross-ambiguity operation between the received DD signal and the pilot signal. There are different energies associated with each DD information signal and the pilot signals[4] [11].

B. Over-the-air Communication

The wireless transmission workflow is as shown in Fig. 3. We generate the TD transmit signal, from Section II-A, using our custom-built Zak-OTFS transmit MATLAB code. This signal is sent from the computer to the transmit side USRP via USB and MATLAB commands. The USRP converts the input signal from baseband to radio frequency (RF) and outputs an RF signal at the specified center frequency. This signal serves as the input of the IF signal to the Tx frontend. We set the LO to the appropriate frequency based on the multiplier and center frequency (approximately 11.7 GHz for the MixAMC and 40 GHz for the CCU/CCD units) of the Tx frontend system. Driven by the LO and IF signals, the Tx frontend upconverts this signal to its associated sub-THz frequency (140 GHz for the MixAMCs and 240 GHz for the CCU/CCD systems). The Tx frontend transmits the upconverted signal over-the air to the Rx frontend. Taking the input LO, the Rx frontend downconverts the received signal and outputs to the receive-side USRP (See Fig. 3) . The USRP downconverts the IF signal to baseband and interfaces with the computer for receive processing. The signal processing described in Section II-B is handled by the custom build Zak-OTFS receive MATLAB code.

C. Zak-OTFS Experiments

To showcase proof-of-concept transmission and reception, we transmitted the two different baseband Zak-OTFS signals (discussed in Section IV-A) over-the-air on the testbed with both the 140 GHz and 240 GHz frontends. We set the distance between the Tx and Rx to a fixed value of 1 m and varied the power by adjusting the internal gain on the USRP; this varies the SNR scenarios under test. For the Zak-OTFS testing with point pilot, we varied the gain between 40-60 dB to collect results for different SNRs, to gain insight on the performance in different channel conditions (noisy versus clear). For the spread pilot OTFS case, we test for a set USRP gain 60 dB and look for the channel prediction along with recovering the overlayed data. Given the stationary, line-of-sight (LOS), set up with no know interferers, we expect a strong LOS component with no reflections. Also, the design of the DD grid is tailored less to the expected channel conditions and more to the hardware limitations.

V. Results

The THz testbed used for the over-the-air experimentation of Zak-OTFS waveform is shown in Fig. 4. The different parameters, both hardware and the Zak-OTFS system parameters, used or the experiments on the THz testbed, are shown in Table I. In this section, we present the results for both data transmission and sensing capabilities of Zak-OTFS system at THz frequencies.

A. Zak-OTFS results with point pilot

We successfully transmitted the Zak-OTFS waveform with point pilot described in Section IV at 140 GHz and 240 GHz RF frontends in three SNR regions: "low" ($\leq$8 dB), "moderate" ($\approx$12 dB), "high" ($\geq$20 dB). Fig. 5 shows the received constellations at 140 GHz for the three SNR regions described above. The bit error rate (BER) obtained in this three SNR regions are: 0.13 at 7.6 dB (low) , 0.05 at 11.6 dB (moderate), and 9.7×10^{-4} at 21.9 dB (high). Also, in Fig. 6, we show the received constellations at 240 GHz for the same three

TABLE I: Zak-OTFS & Hardware Parameters

Parameters	Point Pilot Case	Spread Pilot Case
Base Modulation	QPSK	QPSK
Doppler Period (ν_p)	30 kHz	30 kHz
Delay Period ($\tau_p = 1/\nu_p$)	33.3 μs	33.3 μs
Doppler Taps (N)	48	37
Delay Taps (M)	32	31
Bandwidth (B)	960 kHz	930 kHz
USRP Tx/Rx Gain	Varied	Varied
Tx/Rx Separation	1 m	1 m
IF Frequency	2 GHz	2 GHz
RF Frequencies	140, 240 GHz	140, 240 GHz

[2]For the setup, the channel remains constant for the two OTFS frames.

[3]M, N are even for point pilot case and M, N odd for spread pilot case.

[4]More details on cross-ambiguity and the energies of pilot and data signals are given in [11]

SNR regions and the correspondinf BERs are: 0.16 at 6.8 dB (low) , 0.05 at 12.4 dB (moderate), and no errors at 29.0 dB (high). Of note, our ability to access higher SNR regions with the 140 GHz system is limited by the additional multiplier stage in the hardware compared to the 240 GHz frontends; each multiplier is an additional source of noise, so 140 GHz captures, in-general, tend to be noisier than 240 GHz for the same input power. Therefore, our high-SNR case for 140 GHz is at a lower SNR than the 240 GHz system and has noisier results.

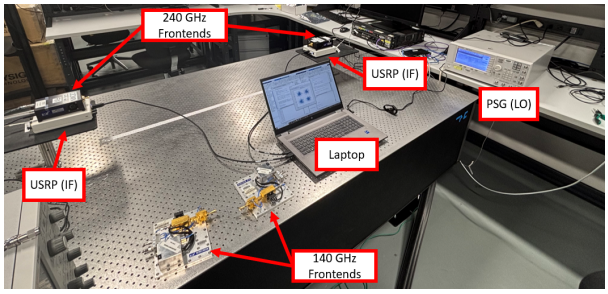

Fig. 4: OTFS on sub-THz laboratory set-up

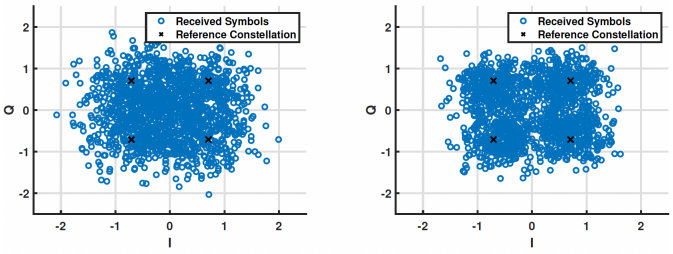

(a) Low SNR (b) Moderate SNR

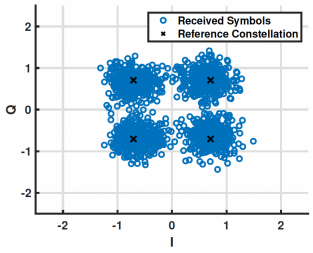

(c) High SNR

Fig. 5: Zak-OTFS constellations at 140 GHz

B. Zak-OTFS results with the spread pilot

As mentioned in Section II-B, to keep the absolute value of the spread pilot constant in all DD resources, we choose $u = 5$ coprime for both M and N (check Table I). With this $u = 5$ and the parameters from Table I, we plot $|x_{\text{s,dd}}[k, l]|$ in Fig. 7(a) for the spread pilot. It can be seen in Fig. 7(a) that all the DD resources have equal/constant spread. Using the signal processing for spread pilot, mentioned in Section IV, the recovered DD signals at 140 GHz and 240 GHz are shown in Fig. 7(b) and Fig. 7(c) respectively. Note that the recovered DD signals, Fig. 7(b) and Fig. 7(c), have data combined with the spread pilot. Using the cross-ambiguity operation, (refer to [11] for details), we first predict the channel response at 140 GHz and 240 GHz using Fig. 7(b) and Fig. 7(c) respectively. The predicted channel responses at 140 GHz and 240 GHz are shown in Fig. 7(d) and Fig. 7(e) respectively. Using this predicted channel, after removing the contribution from the spread pilot, we equalize the effect of the channel on the data. The recovered constellations at 140 GHz and 240 GHz are shown in Fig. 7(f) and Fig. 7(g) respectively. Focusing primarily on the channel prediction result, we observe a strong component centered within the DD grid, with no other significant components. As expected for a stationary LOS set-up, there is no DD shift of the main component into another bin. No observed additional components showcases the lack of reflectors in our setup. Furthermore, we successfully demonstrated data recovery from the ISAC frame. We note a BER of 0.23 for 140 GHz case and BER of 0.01 for 240 GHz (as showcased by the constellations in Fig. 7(f) and Fig. 7(g) respectively). We conducted this with the same USRP gain as our high SNR scenario (60 dB). and find that there are some performance degradations from intertwining the pilot and data within the same frame, however, this can be improved with better decoding. In addition to the sensing

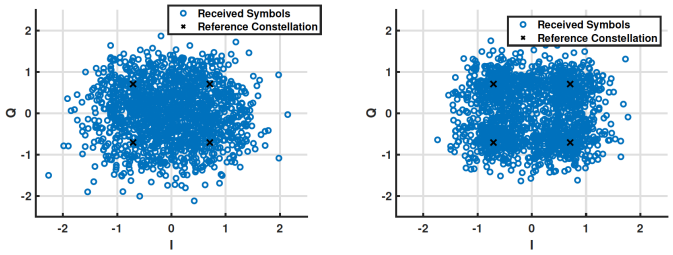

(a) Low SNR (b) Moderate SNR

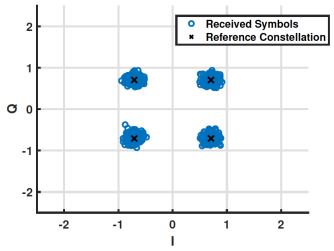

(c) High SNR

Fig. 6: Zak-OTFS constellations at 240 GHz

capability, we measured the PAPR of the point pilot compared to the spread pilot and found a performance improvement of ≈9 dB by using the spread pilot signal (≈15 dB compared to ≈6 dB), which corroborates the results presented in [11]. For the entire signal (pilot and data together), we observe ≈11 dB PAPR for the point-pilot Zak-OTFS signal compared to the ≈6 dB with the spread pilot, which makes ≈5 dB improvement. For sub-THz systems, which are very sensitive to PAPR, this is a promising result.

VI. Conclusion

In this paper, we presented Zak-OTFS with point and spread pilots as potential candidates for next-generation sub-THz

communication systems. We demonstrated both waveforms over-the-air on practical sub-THz wireless communications testbed and evaluated data recovery in a variety of SNR conditions. In addition, we showcased ISAC capabilities and PAPR improvements with spread-pilots. Future work includes more comprehensive BER and SNR measurements to provide a true characterization of performance, as well as tailoring OTFS DD parameters for ultra-wide bandwidths enabled by the sub-THz spectrum.

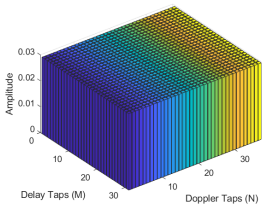

(a) Transmitted pilot

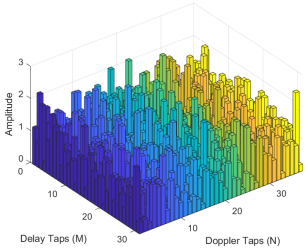

(b) Received pilot 140 GHz

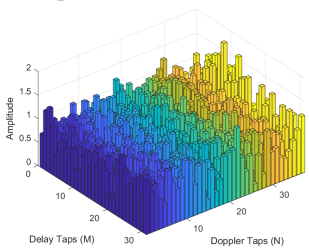

(c) Received pilot 240 GHz

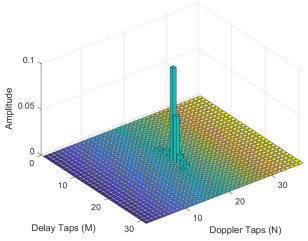

(d) Predicted Channel at 140 GHz

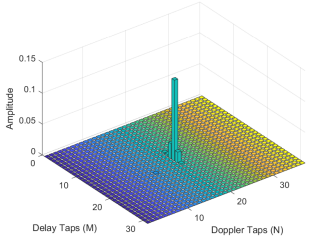

(e) Predicted Channel at 240 GHz

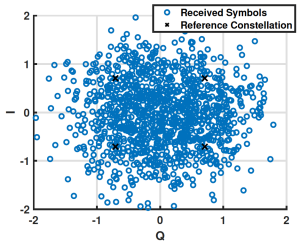

(f) Recovered data 140 GHz

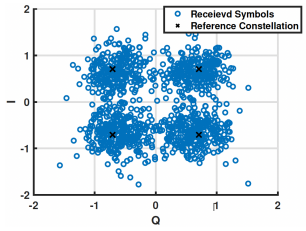

(g) Recovered data 240 GHz

Fig. 7: ISAC for Zak-OTFS with spread pilots.

ACKNOWLEDGMENT

The Duke team is supported by the US National Science Foundation (NSF) (grants 2342690, 2342690, and 214821), in-part by the Air Force Office of Scientific Research (grants FA8750-20-2-0504 and FA9550-23-1-0249), and in-part by federal agency and industry partner funds as specified in the Resilient & Intelligent NextG Systems (RINGS) program. We thank Dr. Saif Khan Mohammed, Jinu Jayachandran from IIT Delhi, India, and Dr. Sandesh Rao Mattu from Duke University, USA, for helping us in this work. Approved for Public Release; Distribution Unlimited: AFRL-2025-1371.

REFERENCES

[1] H. Elayan, O. Amin, B. Shihada, R. M. Shubair, and M.-S. Alouini, "Terahertz band: The last piece of rf spectrum puzzle for communication systems," *IEEE Open Journal of the Communications Society*, vol. 1, pp. 1–32, 2020.

[2] W. Jiang, Q. Zhou, J. He, M. A. Habibi, S. Melnyk, M. El-Absi, B. Han, M. D. Renzo, H. D. Schotten, F.-L. Luo, T. S. El-Bawab, M. Juntti, M. Debbah, and V. C. M. Leung, "Terahertz communications and sensing for 6G and beyond: A comprehensive review," *IEEE Communications Surveys & Tutorials*, vol. 26, no. 4, pp. 2326–2381, 2024.

[3] I. F. Akyildiz, C. Han, Z. Hu, S. Nie, and J. M. Jornet, "Terahertz band communication: An old problem revisited and research directions for the next decade," *IEEE Transactions on Communications*, vol. 70, no. 6, pp. 4250–4285, 2022.

[4] D. Lee, A. Davydov, B. Mondal, G. Xiong, G. Morozov, and J. Kim, "From sub-terahertz to terahertz: challenges and design considerations," in *2020 IEEE Wireless Communications and Networking Conference Workshops (WCNCW)*, pp. 1–8, 2020.

[5] R. Hadani, S. Rakib, M. Tsatsanis, A. Monk, A. J. Goldsmith, A. F. Molisch, and R. Calderbank, "Orthogonal time frequency space modulation," in *2017 IEEE Wireless Communications and Networking Conference (WCNC)*, pp. 1–6, 2017.

[6] S. Tarboush, H. Sarieddeen, M.-S. Alouini, and T. Y. Al-Naffouri, "Single- versus multicarrier terahertz-band communications: A comparative study," *IEEE Open Journal of the Communications Society*, vol. 3, pp. 1466–1486, 2022.

[7] C. T. Parisi, S. Badran, P. Sen, V. Petrov, and J. M. Jornet, "Modulations for terahertz band communications: Joint analysis of phase noise impact and PAPR effects," *IEEE Open Journal of the Communications Society*, vol. 5, pp. 412–429, 2024.

[8] L. Gaudio, G. Colavolpe, and G. Caire, "OTFS vs. OFDM in the presence of sparsity: A fair comparison," *IEEE Transactions on Wireless Communications*, vol. 21, no. 6, pp. 4410–4423, 2022.

[9] Y. Liu, M. Chen, C. Pan, T. Gong, J. Yuan, and J. Wang, "OTFS versus OFDM: Which is superior in multiuser LEO satellite communications," *IEEE Journal on Selected Areas in Communications*, vol. 43, no. 1, pp. 139–155, 2025.

[10] F. Wiffen, L. Sayer, M. Z. Bocus, A. Doufexi, and A. Nix, "Comparison of OTFS and OFDM in ray launched sub-6 ghz and mmwave line-of-sight mobility channels," in *2018 IEEE 29th Annual International Symposium on Personal, Indoor and Mobile Radio Communications (PIMRC)*, pp. 73–79, 2018.

[11] M. Ubadah, S. K. Mohammed, R. Hadani, S. Kons, A. Chockalingam, and R. Calderbank, "Zak-OTFS for integration of sensing and communication," 2024.

[12] S. K. Mohammed, R. Hadani, A. Chockalingam, and R. Calderbank, "OTFS—a mathematical foundation for communication and radar sensing in the delay-doppler domain," *IEEE BITS the Information Theory Magazine*, vol. 2, no. 2, pp. 36–55, 2022.

[13] S. K. Mohammed, R. Hadani, A. Chockalingam, and R. Calderbank, "OTFS—predictability in the delay-doppler domain and its value to communication and radar sensing," *IEEE BITS the Information Theory Magazine*, vol. 3, no. 2, pp. 7–31, 2023.

[14] J. Jayachandran, R. K. Jaiswal, S. K. Mohammed, R. Hadani, A. Chockalingam, and R. Calderbank, "Zak-otfs: Pulse shaping and the tradeoff between time/bandwidth expansion and predictability," 2024.

[15] A. Das, F. Jesbin, and A. Chockalingam, "A gaussian-sinc pulse shaping filter for zak-otfs," 2025.

[16] S. K. Mohammed, R. Hadani, and A. Chockalingam, *OTFS Modulation: Theory and Applications*. Wiley-IEEE Press, 2024.

[17] S. R. Mattu, I. A. Khan, V. Khammammetti, B. Dabak, S. K. Mohammed, K. Narayanan, and R. Calderbank, "Delay-doppler signal processing with zadoff-chu sequences," 2024.

[18] Z. Gao, Z. Qi, and T. Chen, "Mambas: Maneuvering analog multi-user beamforming using an array of subarrays in mmwave networks," ACM MobiCom '24, (New York, NY, USA), p. 694–708, 2024.